Study of Layer Formation during Droplet-based 3D Printing of Gel Structures

Kyle Christensen[1], Yong Huang[1]*

[1]Department of Mechanical and Aerospace Engineering, University of Florida, Gainesville, FL 32611, USA

* Corresponding author, Department of Mechanical and Aerospace Engineering, University of Florida, Gainesville, FL 32611, USA, Phone: 001-352-392-5520, Fax: 001- 352-392-7303, Email: yongh@ufl.edu

Abstract:

Additive manufacturing, also known as three-dimensional (3D) printing, is an approach in which a structure may be fabricated layer by layer. For 3D inkjet printing, droplets are ejected from a nozzle and each layer is formed droplet by droplet. Inkjet printing has been widely applied for the fabrication of 3D biological gel structures, but the knowledge of the microscale interactions between printed droplets is still largely elusive. This study aims to elucidate the layer formation mechanism in terms of the formation of single lines and layers comprised of adjacent lines during drop-on-demand inkjet printing of alginate using high speed imaging and particle image velocimetry. Inkjet droplets are found to impact, spread, and coalesce within a fluid region at the deposition site, forming coherent printed lines within a layer. The effects of printing conditions on the behavior of droplets during layer formation are discussed and modeled based on gelation dynamics, and recommendations are presented to enable controllable and reliable fabrication of gel structures. The effects of gelation on droplet impact dynamics are found to be negligible during alginate printing, and interfaces are found to form between printed

lines within a layer depending on printing conditions, printing path orientation, and gelation dynamics.

Keywords: Bioprinting, inkjet printing, line formation, layer formation, droplet deposition

1. Introduction

Additive manufacturing (AM), also known as three-dimensional (3D) printing, is an approach in which material is deposited in specified two-dimensional (2D) patterns to build 3D parts layer by layer. This has been accomplished through numerous technologies including material extrusion, powder bed fusion, vat photopolymerization, and material jetting, to name a few [1]. In general, AM offers unparalleled design flexibility and potential for the fabrication of complex user-defined parts and structures on demand. 3D bioprinting is one promising application of AM technology [2-8], aiming to fabricate structures for use in regenerative medicine, pharmacokinetic, and cell biology studies [1,9,10]. For 3D bioprinting, a structure is typically built layer-by-layer by the deposition of biomaterials and living cells into prescribed geometries based on a designed 3D model. This approach offers potential for the fabrication of heterogeneous, geometrically-relevant biological structures to effectively mimic the function of native tissues [11], which is central to the advancement of tissue engineering and regenerative medicine [12-14]. Continued advancement toward the fabrication of transplantable organs is of utmost concern [15], as thousands of lives are lost each year awaiting transplants in the United States alone [16].

Most bioprinting processes typically involve two key steps: material deposition and solidification/gelation. Material deposition may be accomplished by material extrusion [17-20]

or material jetting, which includes laser-induced forward transfer (LIFT) [6,7,21] and inkjetting [2,4,5]. After deposition, biomaterial solidification can be initiated by various mechanisms including light-induced curing [22,23], ionic crosslinking [5,7], and thermal gelation [20], to name a few. Of various material deposition technologies, droplet-based material jetting is often favored for its low cost, high speed, and high resolution [24]. To form 3D parts using material jetting, precursor droplets are deposited and they coalesce into defined 2D layers before being solidified. Typically, printed droplets impact and coalesce with previously deposited material to form coherent lines and layers. Herein, a commonly applied case of material jetting is studied in which hydrogel structures are fabricated layer-by-layer due to ionic gelation as they are submerged into a crosslinking and supporting solution [2,4,5,7]. Deposited droplets coalesce to form a layer of designed shape, and the structure is then lowered by the layer thickness into a solution to facilitate crosslinking. However, the layer formation process during this droplet-based material jetting approach is not yet well understood.

The objective of this study is to characterize the effects of printing and gelation conditions on the layer formation process and resulting morphology of 3D inkjet printed structures for droplet-based inkjet printing of alginate solutions. An improved understanding of the layer formation process is expected to enable better control of the printing process, which may lead to improved part quality and process reliability. While an ionic gelation-enabled inkjetting approach is studied herein, the fundamental understanding of droplet impact, coalescence, and solidification during layer formation is relevant to other material jetting-based AM processes.

2. Background

The fabrication of high quality end-user products by AM demands both dimensional accuracy and surface finish quality in printed parts [25-27]. Knowledge of the relationships between printing conditions and resulting part quality ultimately improves AM capabilities. In particular, understanding the interaction of printed droplets and the subsequent formation of layers is critical to the success of droplet-based approaches. While several studies have demonstrated the macroscopic formation of structures using droplet-based printing [2-8], little has been presented regarding the microscopic interactions between droplets and subsequent formation of layers. The formation of inkjet-printed lines onto a solid substrate [28] or a liquid bath [4] has been studied. However, conditions were not fully representative of the layer formation process during the fabrication of 3D structures. Similarly, the morphologies of lines laser printed onto a glass substrate have been observed [8] but again do not fully represent conditions occurring during structure fabrication. The layer formation process during structure fabrication depends on the effects of simultaneous gelation as well as the interaction between adjacent printed lines, such that further investigation is required.

Layer formation during inkjet printing has been studied for the fabrication of microvasculature-like structures using a small droplet diameter (50 μm) and comparatively low printing frequency (4.9 Hz) [29]. Printing micrometer-scale droplets at such a low frequency causes each printed droplet to be individually gelled, preventing coalescence with adjacent droplets as planned by the authors. This approach results in segmented layers with distinct boundaries between droplets which affects the mechanical strength and integrity of the structure due to the discernable interfaces between adjacent droplets and lines. Conversely, the formation of continuous lines and coalescence of adjacent lines within a printed layer may improve the

mechanical properties and geometric fidelity of printed structures and should be carefully examined.

The impact, coalescence, and gelation of droplets during the formation of a layer are analyzed using high speed imaging, particle image velocimetry (PIV), and microscopic measurements from printed layers. PIV is a noncontact measurement approach for determining the displacement and velocity fields of particles embedded within a moving fluid over time. Of numerous applications, PIV has been used to determine velocity fields within microfluidic junctions [30-32] and microscale droplets [33-35]. As such, PIV is appropriate for observing the behavior of droplets during impact and coalescence to better understand the layer formation process during droplet-based printing.

3. Inkjet Printing and Experimental Design

3.1. Inkjet Printing Setup and Materials

As shown in Fig. 1(a), a previously described platform-assisted 3D inkjet printing system [5] was implemented as the enabling bioprinting technology. For 3D structure fabrication, layers are formed as droplets of a precursor solution are deposited via a piezoelectric printhead onto a substrate maintained at the surface of a crosslinking and supporting solution. The deposition location along designed 2D patterns is controlled by computerized *XY* motion stages which move the printhead along a printing path comprised of printed lines and feeds between lines. While not necessary for the fabrication of single layers detailed herein, multiple layers are deposited consecutively onto one another as the structure is lowered into the crosslinking and supporting solution. Crosslinking of deposited layers occurs by ion diffusion from the surrounding solution and previously-printed layer, forming a mechanically stable hydrogel.

Herein droplets were generated on-demand from an MJ-ABL piezoelectric inkjet printhead (MicroFab, Plano, TX) with a 120 μm diameter orifice. The printhead was driven by a bipolar waveform with ±80 V potential, 3 μs rise and fall times, and 45 μs dwell and echo times at a frequency of 60 Hz via a JetDrive III controller (MicroFab, Plano, TX). The printhead was mounted to a set of motorized linear *XY* stages (Aerotech, Pittsburgh, PA) and the receiving substrate was mounted to a separate motorized linear Z stage (Aerotech, Pittsburgh, PA). The *XY* printing path of the printhead and *Z*-direction submersion of the substrate were coordinated using AeroBasic and G-code commands developed in-house based on the desired geometry. Printhead travel speeds of 1.8 mm/s for PIV analysis and 3.3 mm/s for full layer fabrication were used with ejection frequency of 60 Hz; the resulting droplets were approximately 100 μm in diameter as measured using a typical time-resolved imaging setup [4]. These printing conditions are representative of those for typical structure fabrication by inkjet printing [4,5]. A printhead travel speed of 1.8 mm/s was chosen during high speed imaging and PIV to reduce the distance between adjacent deposited droplets and enable a smaller field of view and higher magnification to better examine the details of droplet dynamics during impact and coalescence. A printhead travel speed of 3.3 mm/s was chosen during the layer formation study to illustrate the scenario of well-defined regions of coalescence as well as interfaces during the fabrication of a single layer.

Sodium alginate and calcium chloride were chosen as they are the most common solution pairing used in droplet-based printing due to good availability, desirable mechanical properties, and a high rate of gelation [2-8]. The printed solution consisted of 1% (w/v) sodium alginate (Sigma-Aldrich, St. Louis, MO) solution prepared in deionized (DI) water and was laden with white polystyrene beads (15 μm diameter, Polysciences, Warrington, PA) to enable the use of PIV, as detailed in a subsequent section. The crosslinking and supporting solution consisted of

2% (w/v) calcium chloride dihydrate ($CaCl_2$) prepared in DI water. Alginate undergoes gelation when it interacts with multivalent cations such as Ca^{2+}. Gelation occurs as the Ca^{2+} cations take part in the interchain ionic bonding between G blocks in the polymer chain, giving rise to a stable hydrogel network of calcium alginate.

3.2. Experimental Design

3.2.1. Design of Printing Experiments

The formation of individual layers is fundamental for the fabrication of 3D structures as shown in Fig. 1(a). However, the ability to observe the formation of a layer during a typical supporting/crosslinking fluid-enabled inkjet printing process is very limited. Macroscopic structures consisting of multiple layers lose their translucence, and discerning between individual layers becomes challenging. In order to closely examine the formation of alginate layers, a single layer was printed onto a prefabricated gelled alginate sheet. This experimental scenario (Scenario A as shown in Fig. 1(b)) accurately recreates the typical fabrication process as a newly deposited layer is printed onto a gelled alginate layer, and gelation of the new layer occurs via diffusion through the previous layer at the surface of the surrounding $CaCl_2$. Thin alginate sheets approximately 1 mm in thickness were prepared by casting 1% (w/v) sodium alginate and facilitating gelation with 2% (w/v) $CaCl_2$. These sheets were kept hydrated with 2% (w/v) $CaCl_2$ and a single layer was printed on top, while the transparency allowed for imaging during printing and microscopic measurements after printing. The hydrated substrates in Fig. 1(b) mimic the transfer of calcium ions due to both the $CaCl_2$ bath present in normal printing as well as by diffusion through the a previously printed gelled layer. Additionally, the gel substrate provides a soft elastic and wetted surface for droplet impact and spreading, as is present under normal

printing conditions. Scenario A was implemented to study the formation of lines, interfaces between lines within a layer, and process modeling during inkjet printing.

In addition, another experimental scenario (Scenario B as shown in Fig. 1(c)) was designed to improve the visualization of interfaces between printed lines. A bath of 2.4% (w/v) Laponite RD (BYK Additives Inc., Austin, TX) was prepared containing 2% (w/v) $CaCl_2$, and a layer was inkjet printed directly into the Laponite bath. The chosen Laponite concentration enables representative layer formation as deposited droplets penetrate a short distance into the solution and are held in place as a layer due to the yield-stress behavior of the Laponite bath. Printing occurred within one hour of preparing the bath as Laponite was found to lose its yield-stress properties after several hours when mixed with $CaCl_2$. The Laponite bath supported the layer during fabrication and facilitated crosslinking via diffusion, and the printed layer can be further isolated for imaging by removing surrounding Laponite by sonication. While Scenario B enables isolation of single printed layers for improved visualization presented herein, all quantitative experimental data was determined using Scenario A.

3.2.2. Study of Liquid Coalescence using High Speed Imaging and PIV

The high speed imaging apparatus illustrated in Fig. 2 was implemented along with PIV analysis in a manner similar to a previous study [34] to visualize and quantify the coalescence of printed droplets during the layer formation process. A vertically oriented Fastcam SA5 (Photron, San Diego, CA) high speed camera recorded motion at 5,000 frames per second with a shutter speed of 50 μs. This framerate and shutter speed combination was selected to give adequate brightness and time between frames with very little blurring or distortion. Droplets are deposited

onto a gelled alginate substrate surrounded by a $CaCl_2$ solution (Scenario A) placed onto a transparent glass slide above the camera.

PIV enables visualization and quantification of fluid flow by comparing the relative location of suspended tracer particles between images captured over a known time interval. Images of the formation of printed lines were captured by high speed imaging. PIV analysis was completed using PIVlab [36]. White polystyrene beads were added to a 0.5% sodium alginate solution as tracer particles for PIV analysis to a final concentration of 3.375×10^6 beads/mL, or a volume fraction of 0.6%. This concentration was determined experimentally and found to offer a densely packed high contrast pattern suitable for PIV. The effects of the beads on fluid flow is assumed to be negligible due to the short time scale, high flow velocity, and disinterest in flow close to a boundary wall [37]. A high intensity LED was oriented nearly coaxially to the printhead and camera, such that there was a strong contrast between beads and the surrounding solution. Due to the low thickness of the spreading droplet and fluid region as well as the disinterest in flow at the perimeter of the fluid, the effects of refraction on PIV data are considered negligible [34] and motion is assumed to be almost entirely in the plane of imaging.

PIV was used to visualize and quantify two-dimensional fluid flow during droplet impact and coalescence within a printed line. A printhead travel speed of 1.8 mm/s, ejection frequency of 60 Hz, and droplets of 100 μm diameter were used herein which are representative of typical fabrication by inkjet printing [4,5]. While variations in printing conditions affect measured values, the overall behavior and layer formation process observed is representative of a range of typically utilized printing conditions. The maximum framerate which provided ample lighting and blur reduction was found to be 5,000 frames per second, leading to a lapse of 200 μs between successive images.

4. Investigation of Layer Formation Process

Each layer within a 3D-printed structure is composed of a series of printed lines, where material is deposited along a certain designed printing path as illustrated in Fig. 3. During inkjet printing, each line is formed by continuously deposited droplets. Once a droplet is formed, it travels through air and lands onto a receiving substrate. For typical macroscopic structure fabrication, each droplet impacts, spreads, and coalesces with previously printed material to form seamless printed lines without discernable interfaces or borders between adjacent droplets. At the same time, gelation occurs continuously during this ionic crosslinking-based fabrication process. This approach varies notably from a related inkjet printing layer formation study in which the rate of material deposition was deliberately low compared to that of material gelation, such that each droplet was gelled before subsequent droplets were deposited [29].

The rate of droplet deposition compared to the nozzle travel speed under typical conditions is such that each droplet lands partially overlapping with the previous droplet, as indicated by the overlap distance shown in Fig. 3. Due to the spread of fluid from previously printed droplets, droplets land on a fluid region at the impact site. Herein the layer formation investigation aims to better understand the behavior of material during the formation of a printed layer to help ensure a repeatable and controllable printing process.

4.1. Study of Single Line Formation

4.1.1. Droplet Impact and Coalescence

Figure 4 shows top view PIV results during droplet impact and coalescence as a line is printed. The droplet impact center can be seen at $t = 0$ μs (Fig. 5(a)) as the droplet first lands and

displaces fluid from previously printed droplets within the line. A high velocity region is observed to a radius of 150 μm (3 times the droplet radius) 200 μs after impact as the droplet spreads. Fluid displacement is generally symmetrical and largely directed radially outward from the impact location as the droplet spreads, and a ripple which travels throughout the fluid region is created. The ripple within the fluid is observed to travel to a radius of 200 μm (4 times the droplet radius) 400 μs after impact (Fig. 5(b)). The distribution takes on an annular shape, where high velocity remains toward the exterior of the initial 150 μm radius, but a decrease in the velocity is measured toward the impact center as the fluid from the deposited droplet reaches equilibrium. By 600 μs (Fig. 5(c)), the measured velocity within the entire disturbed region up to 200 μm from the impact center has decreased sharply and become nearly uniform. Measured velocity continues to decrease uniformly within the disturbed region by 800 μs as the impact energy is dissipated and coalescence completes.

The evolution of the average velocity at a given radius (82 μm) over time is plotted in Fig. 5, and this radius is selected based on the highest average velocity at 400 μs when the highest maximum velocity is observed for the entire impact process. To capture an average velocity, 300 points evenly spaced around any radius are measured and averaged. The velocity magnitude at this radius (82 μm) is seen to first increase as droplet impact and spreading occurs, then decrease as energy is dissipated. The standard deviation represented by error bars (one standard deviation) in Fig. 5 indicates a somewhat large variation at 200 and 400 μs time points due to radial asymmetry in the impact and imperfections in the imaging and PIV analysis.

The velocity magnitude increases quickly over the first 200 μs as the droplet impacts and spreads. The velocity magnitude increases at a much slower rate from 200-400 μs as droplet spreading completes and reaches its peak measured value. The velocity magnitude then

decreases very quickly from 400-600 μs as energy is transferred to surrounding fluid and impact and coalescence is nearly completed. Velocity continues to decrease gradually due to damping from 600 to 1000 μs and the fluid reaches equilibrium well before the subsequent droplet is deposited when the droplet deposition frequency is 60 Hz (16,666 μs between impacts).

Droplet behavior when impacting a fluid region may result in bouncing, coalescence, and/or splashing [38]. No splashing or bouncing was observed herein, which should be avoided to ensure the reliable formation of printed lines. Droplet spread and coalescence occurred in a manner typical for impact with a fluid region [39,40]. Material at the landing site flows mostly radially outward as the droplet spreads and displaces fluid after impact (t = 0-200 μs) as shown in Fig. 5(b). Velocity vectors are then directed radially inward as the droplet retracts and any resulting crater in the surrounding fluid is filled and leveled (t = 400-600 μs). Vector directions which are not radial and variations in velocity magnitude may be attributed to vortexes, which have been observed for droplets impacting a fluid [38].

The impact of droplets onto a receiving substrate is of importance in many engineering applications including inkjet printing. Depending on the kinetic energy level of jets/droplets during impact, there might be three outcomes: spreading to form a lamella, rebounding off the surface, or splashing. Spreading and splashing commonly occur during inkjet printing of viscoelastic solutions such as the alginate solution in this study. Jets/droplets with low kinetic energy result in spreading while jets/droplets with high kinetic energy lead to splashing, which should be avoided for better printing quality. Generally, the Weber number ($We = \rho v_d^2 d/\sigma$), where ρ is the fluid density, v_d is the droplet impact velocity, d is the characteristic length, and σ is the surface tension, is used to examine the occurrence of splashing. A Weber number represents the ratio of the liquid inertia to surface tension effects during impact. Splashing may

occur if the Weber number is higher than a critical Weber number. In this study, the Weber number is 28.8 with ρ of 1 g/mL, v_d of 3.7 m/s, d of 100 μm which is taken as the droplet diameter, and σ of 47.5 mN/m as measured. The Weber number herein is much smaller than the critical Weber number for splashing during jet-based printing of alginate solutions, which is on the order of 1000 [41]. High speed imaging and PIV analysis have shown that there is no splashing or bouncing, and droplet impact, spreading, and coalescence is well-defined and repeatable under the conditions herein. Specifically, the inertia of impact is not high enough compared to surface tension effects such that splashing is prevented [42] due to viscous damping and coalescence with the surrounding fluid; bouncing is prevented and coalescence of a printed droplet within the fluid region is facilitated as the energy of impact is sufficient to expel the air film between the droplet surfaces [43].

4.1.2. Gelation Process

A simple one-dimensional (1D) gelation model has been applied to predict the advancement of a gelation front through the thickness of a printed line [7]. The 1D gelation model utilized is based on the kinetic study of calcium alginate in which a reaction front advances through a layer based on the diffusion process and reaction stoichiometry [44]. The position of the gelation front $G(t)$ through the thickness of the layer h over time t can be estimated by Equation (1) [45]. As illustrated in Fig. 6, the primary source of free ions for the gelation of newly deposited material is considered to be in contact with the gelled alginate sheet onto which the layer is printed. This neglects the fact that ion diffusion occurs from the adjacent printed and gelled lines within a layer. This minor source of diffusion can be reasonably

neglected as the free ion concentration is considerably lower than that of the gelled alginate sheet soaked in $CaCl_2$ and acts only along the layer thickness rather than the printed line width.

Herein, the bulk concentration of the printed alginate solution a_0 is 0.1 mol L^{-1} for 1% alginate and the guluronic acid content G has been reported as 70% [46]. The diffusion coefficient of free calcium ions D_c is interpolated as 0.77×10^{-9} m^2s^{-1} [47] for calcium cations with a bulk concentration C_0 of 0.136 mol L^{-1} for 2% (w/v) $CaCl_2\bullet2H_2O$ solution. The shorthand notation of the calcium cation bulk concentration is defined as $\theta = \frac{C_0}{N_c a_0}$ [45] where the stoichiometric calcium cation binding capacity is $N_c = \frac{3}{4}G$ [48]. The equivalent filter length for the reaction-diffusion model L_d is taken as 0 in this case as the alginate sheet onto which printing occurs is submerged up to its surface in $CaCl_2$.

$$G(t) = \sqrt{2D_c\theta t + L_d^2} - L_d \tag{1}$$

Equation (1) predicts that the timescale for gelation through the full thickness of the printed layer is 690 ms. High speed imaging and PIV has revealed that the timescale for droplet impact and coalescence is on the order of 600 μs under the conditions used herein, or three orders of magnitude shorter. Equation (1) predicts that less than 1.7 μm, or 3% of the line thickness, is gelled over 600 μs. Since droplet impact and coalescence is nearly complete by 600 μs, gelation effects during the impact and coalescence of droplets within a printed line are considered to be negligible in this study. The relatively long predicted timescale for gelation also supports the observation that droplets interact in a fluid region at the deposition location. At a deposition frequency of 60 Hz, 16.7 ms elapse between droplet impacts. This time is substantially shorter than that required for the gelation of the printed line.

4.2. Study of Layer Formation

4.2.1. Geometry of Printed Features

A printed line within a layer is formed by a single linear motion of the printhead as it continuously deposits droplets. From a cross sectional view, a slightly bowed surface has been observed at the top of each printed line due to surface tension effects. However, curvature is assumed to be mostly negligible under typical printing conditions and the cross-sectional shape of each line is approximated as a rectangle herein. As such, Equation (2) simply based on the volume constancy represents the average layer thickness h for a given line width w, deposition frequency f, droplet diameter d_D, and printhead velocity v_{print}.

$$h = \frac{\pi f d_D^3}{6 w v_{print}} \tag{2}$$

For layer formation studies, layers were printed with a droplet diameter of 100 μm as measured by stroboscopic imaging, continuous deposition frequency of 60 Hz, a printhead velocity of 3.3 mm/s, and a designed line width (feed distance between printed lines) of 0.17 mm. The feed speed was 10 mm/s and droplets deposited during feeds are assumed to have a negligible effect on layer formation due the high printhead velocity and short feed distance, such that a negligible number of droplets are deposited during the feed [49]. These printing conditions are typical for inkjet printing and result in well-defined layers while offering a high rate of material deposition and thus a low fabrication time for structures. Equation (2) predicts a layer thickness of 56 μm using these conditions. Actual layer thickness is determined as approximately 50 μm from microscopic inspection of fifty-layer tubular structures, which is in good agreement with the predicted value. The slight discrepancy can likely be attributed to material shrinkage during gelation and measurement inaccuracy.

The prediction of printed line geometry is necessary for the effective design and fabrication of 3D structures. While there is no direct control of the width or thickness of a printed line for given printhead nozzle diameters and printhead travel speeds as the spread of deposited material depends on the material viscosity, surface tension, and jet velocity, the printed line width is somewhat constrained by the printing path design. That is, the designed distance between adjacent printed lines determines the maximum width of each line as the previous and subsequently printed lines act as barriers to prevent spreading. If lines are too far apart, gaps in the material exist and a coherent layer is not formed. Similarly, if lines are too close together there will be material overflow and nonuniform buildup. The resulting line width determines the thickness of each layer, a key parameter when fabricating structures by additive manufacturing.

4.2.2. Formation of Adjacent Lines

For typical fabrication of a layer, a printing path consists of a series of parallel and adjacent lines with a printhead depositing material along these lines. As such, the formation of adjacent lines within a layer is of concern for the fabrication of 3D structures. Between any adjacent lines printed at speed v_{print} with print distances d_{print}, the printhead travels a short feed distance d_{feed} (feed distance between adjacent lines) at a high speed v_{feed} (the printhead feed speed) during which a negligible amount of material is deposited such that a layer can be formed by a continuous serpentine path [49]. Within the resulting printed layer as shown in Fig. 7(a), distinct interfaces may exist between printed lines in certain regions while printed lines in other regions coalesce entirely. For the inset shown in Fig. 7(a), there is a large time lapse Δt between the deposition of adjacent regions in printed lines L1 and L2 (forming an interface) while there is a small Δt between the deposition of adjacent regions in printed lines L3 and L4 (no interface

formed). This results in the formation of interfaces between adjacent lines depending on Δt between the deposition of two adjacent lines. Furthermore, whether two lines coalesce or form an interface is dependent on the gelation state of contacting materials between adjacent lines, which depends on Δt. If material from one printed line is still fluid or partially fluid when an adjacent line is deposited, the lines coalesce and no visible interface is formed. Conversely, if material from one printed line is fully gelled before an adjacent line is deposited, an interface is formed instead of coalescence. It is noted that partial coalescence in which an interface exists through part of the layer thickness and the remainder is coalesced is considered the same as full coalescence. It is difficult to distinguish between partial and full coalescence using microscopic imaging due to the lack of a defined visible interface. Thus, only the cases of coalescence (no visible interface) and the full prevention of coalescence (visible interface) are considered herein.

Using the prediction of the distance the advancing gelation front travels throughout the printed layer over time from Equation 1, comparisons can be drawn based on the time which passes before the coalescence of two adjacent lines is prevented. Dependent on printing conditions, the time passing before the formation of an interface is straightforward to determine from experimental observations across printed samples. For seamless layer formation which has completely coalesced adjacent lines, it is required that the time between printing adjacent lines is less than the maximum time lapse facilitating coalescence, Δt_{max}. This time is represented by Equation (3) where the coalescence distance L is the measured distance from the edge of a layer to the beginning of the interface, i.e. the distance between two lines in which coalescence occurs, d_{feed} is the feed distance between adjacent lines, and v_{feed} is the printhead feed speed.

$$\frac{2L}{v_{print}} + \frac{d_{feed}}{v_{feed}} \leq \Delta t_{\max} \tag{3}$$

Across multiple samples printed using conditions mentioned previously, the average time passing before the formation of an interface was found to be 690 ms with a standard deviation of 120 ms. Figure 9 plots this time point along with the predicted distance that the gelation front travels over time using Equation (1). The predicted layer thickness of 56 μm using Equation (2) is plotted for comparison. A layer thickness of 50 μm measured from a macroscopic structure printed under identical printing conditions is also plotted, and is representative of the thickness of the single printed layer. It can be seen that within one standard deviation, the point of prevented coalescence as shown in Fig. 9 coincides with the advancement of the gelation front through the entire thickness of the sheet based on predicted and measured values. This supports the conclusion that as the advancing gelation front reaches the top or near the top of the printed layer, i.e. the material within the line is fully gelled, coalescence will be prevented and an interface will be formed as seen from Fig. 7.

5. Conclusions

An experimental setup which is representative of typical fabrication conditions is implemented and enables the use of high speed imaging and PIV to study the layer formation process during inkjet printing of gel structures. Printed droplets are found to impact and coalesce within a fluid region under typical conditions, enabling the fabrication of well-defined lines without discernable interfaces between droplets. To facilitate coalescence within printed lines, the droplet deposition rate should be high compared to the rate of gelation. That is, the time between the deposition of adjacent droplets should be much smaller than the time required for the gelation of each droplet. Herein, PIV and a 1D gelation model indicate that the timescale for droplet impact and coalescence is three orders of magnitude shorter than the timescale for

complete gelation of a printed line. That is, the timescale for droplet impact, spreading, and coalescence is significantly shorter than the timescale for gelation of a layer, such that the effects of gelation on droplet impact dynamics are negligible during alginate printing. The rate of droplet deposition should be maximized, which additionally reduces the time to fabricate a structure or pattern. However, the gelation rate should be high enough to ensure full gelation of each layer before subsequent layers are deposited.

The formation of interfaces between adjacent lines within a layer may or may not occur depending on the printing parameters, print path orientation, and gelation dynamics. While no interfaces are observed between droplets within a printed line, distinct interfaces are observed between printed lines within a layer under typical printing conditions. The formation or prevention of these interfaces is found to be dependent on the time lapse between the deposition of adjacent regions. The 1D gelation model predicts that the maximum time lapse facilitating coalescence reasonably coincides with the time required for full-thickness gelation of a printed line. For coherent layers without interfaces, the time between the deposition of any adjacent regions using a serpentine path should be less than the maximum time lapse.

This study helps understand the layer formation mechanisms for inkjet fabrication of gel structures in terms of the gelation effects on droplet impact dynamics and the formation of line interfaces as a function of printing parameters, print path orientation, and gelation dynamics. Such understanding aids in the selection of printing parameters for reliable and controllable layer-by-layer fabrication of 3D structures without material inconsistencies such as interfaces. However, interfaces between printed lines are formed under certain printing conditions and may affect the mechanical stiffness and fracture strength of printed gel structures. Such effects are dependent on the interface orientation with respect to an applied load and are to be further

characterized in a future study. Other future work may include the statistical analysis of the impact/coalescence process of droplets, the characterization of the effects of hydrogel swelling and dehydration on the presence of interfaces, the examination of the range of Weber number as well as other applicable dimensionless numbers to better qualify the impact/coalescence process, the verification of the effects of improved process planning on the mechanical strength and geometric fidelity of printed parts, and the study of layer formation mechanisms for approaches other than inkjet printing.

Acknowledgements

This work was partially supported by the US National Science Foundation (NSF CMMI-1634755). The discussion with Ruitong Xiong on the gelation modeling is highly appreciated.

References

[1] Huang, Y., Leu, M.C., Mazumder, J., and Donmez, A., 2015, "Additive Manufacturing: Current State, Future Potential, Gaps and Needs, and Recommendations," Journal of Manufacturing Science and Engineering, **137**, 014001.

[2] Boland, T., Tao, X., Damon, B.J., Manley, B., Kesari, P., Jalota, S., and Bhaduri, S., 2007, "Drop on Demand Printing of Cells and Materials for Designer Tissue Constructs," Mat. Sci. Eng. C, **27**, pp. 372-376.

[3] Nishiyama, Y., Nakamura, M., Henmi, C., Yamaguchi, K., Mochizuki, S., Nakagawa, H., and Takiura, K., 2009, "Development of a Three-dimensional Bioprinter: Construction of Cell Supporting Structures Using Hydrogel and State-of-the-art Inkjet Technology," J. Biomech. Eng., **131**, 035001.

[4] Xu, C., Chai, W., Huang, Y., and Markwald, R.R., 2012, "Scaffold-free Inkjet Printing of Three-dimensional Zigzag Cellular Tubes," Biotechnol. Bioeng., **109**, pp. 3152–3160.

[5] Christensen, K., Xu, C., Chai, W., Zhang, Z., Fu, J., and Huang, Y., 2015, "Freeform Inkjet Printing of Cellular Structures with Bifurcations," Biotech. Bioeng., **112**, pp. 1047-1055.

[6] Yan, J., Huang, Y., and Chrisey, D.B., 2013, "Laser-assisted Printing of Alginate Long Tubes and Annular Constructs," Biofabrication, **5**, 015002.

[7] Xiong, R., Zhang, Z., Chai, W., Huang, Y., and Chrisey, D.B., 2015, "Freeform Drop-on-demand Laser Printing of 3D Alginate and Cellular Constructs," Biofabrication, **7**(4), 045011.

[8] Xiong, R., Zhang, Z., and Huang, Y., 2015, "Identification of Optimal Printing Conditions for Laser Printing of Alginate Tubular Constructs," Journal of Manufacturing Processes, **20**, pp. 450-455.

[9] Horch, R.E., 2006, "Future Perspectives in Tissue Engineering," J. Cell. Mol. Med., **10**(1), pp. 4-6.

[10] Ringeisen, B.R., Othon, C.M., Barron, J.A., Young, D., and Spargo, B.J., 2006, "Jet-based Methods to Print Living Cells," Biotechnol. J., **1**(9), pp. 930-948.

[11] Tsang, V.L., and Bhatia, S.N., 2004, "Three-dimensional Tissue Fabrication," Advanced Drug Delivery Reviews, **56**, pp. 1635-1647.

[12] Kolesky, D.B., Truby, R.L., Glagman, A.S., Busbee, T.A., Homan, K.A., and Lewis, J.A., 2014, "3D Bioprinting of Vascularized, Heterogeneous Cell-laden Tissue Constructs," Adv. Mater., **26**(19), pp. 3124-3130.

[13] Colosi, C., Shin, S.R., Manoharan, V., Massa, S., Costantini, M., Barbetta, A., Dokmeci, M.R., Dentini, M., and Khademhosseini, A., 2015, "Microfluidic Bioprinting of

Heterogeneous 3D Tissue Constructs Using Low-Viscosity Bioink," Adv. Mater., **28**(4), pp. 667-684.

[14] Kang, H., Lee, S.J., Ko, I.K., Kengla, C., Yoo, J.J., and Atala, A., 2016, "A 3D Bioprinting System to Produce Human-scale Tissue Constructs with Structural Integrity," Nature Biotechnology, **34**(3), pp. 312-319.

[15] Abouna, G.M., 2008, "Organ Shortage Crisis: Problems and Possible Solutions," Transplantation Proceedings, **40**, pp. 34-38.

[16] http://www.organdonor.gov/about/data.html, accessed Nov. 2016.

[17] Norotte, C., Marga, F. S., Niklason, L. E., and Forgacs, G., 2009, "Scaffold-Free Vascular Tissue Engineering Using Bioprinting," Biomaterials, **30**, pp. 5910-5917.

[18] Skardal, A., Zhang, J., and Prestwich, G. D., 2010, "Bioprinting Vessel-Like Constructs Using Hyaluronan Hydrogels Crosslinked with Tetrahedral Polyethylene Glycol Tetracrylates," Biomaterials, **31**, pp. 6173-6181.

[19] Duan, B., Hockaday, L., Kang, K., and Butcher, J., 2012, "3D Bioprinting Heterogeneous Aortic Valve Conduits with Alginate/Gelatin Hydrogels," J. Biomed. Mater. Res. Part A, **101A**, 025016.

[20] Jin, Y., Compaan, A., Bhattacharjee, T., and Huang, Y., 2016, "Granular Gel Support-enabled Extrusion of Three-dimensional Alginate and Cellular Structures," Biofabrication, **8**(2), 025016.

[21] Riggs, B.C., Dias, A.D., Schiele, N.R., Cristescu, R., Huang, Y., Corr, D.T., and Chrisey, D.B., 2011, "Matrix-assisted Pulsed Laser Methods for Biofabrication," MRS Bull., **36**(12), pp. 1043-1050.

[22] Hockaday, L.A., Kang, K.H., Colangelo, N.W., Cheung, P.Y.C., Duan, B., Malone, E., Wu, J., Girardi, L.N., Bonassar, L.J., Lipson, H., Chu, C.C., and Butcher, J.T., 2012, "Rapid 3D Printing of Anatomically Accurate and Mechanically Heterogeneous Aortic Valve Hydrogel Scaffolds," Biofabrication, **4**, 035005.

[23] Hoch, E., Hirth, T., Tovar, G.E.M., and Borchers, K., "Chemical Tailoring of Gelatin to Adjust Its Chemical and Physical Properties for Functional Bioprinting," 2013, J. Mater. Chem. B, **1**, pp. 5675-5685.

[24] Murphy, S.V., and Atala, A., 2014, "3D Bioprinting of Tissues and Organs," Nature Biotechnology, **32**(8), pp. 773-785.

[25] Ippolito, R., and Iuliano, L., 1995, "Benchmarking of Rapid Prototyping Techniques In Terms Of Dimensional Accuracy and Surface Finish," Annals of the CIRP, **44**(1), pp. 157-160.

[26] Armillotta, A., 2006, "Assessment of Surface Quality on Textured FDM Prototypes," Rapid Prototyping Journal, **12**(1), pp. 35-41.

[27] Galantucci, L.M., Lavecchia, F., and Percoco, G., 2009, "Experimental Study Aiming to Enhance the Surface Finish of Fused Deposition Modeled Parts," Manufacturing Technology, **58**, pp. 189-192.

[28] Stringer, J., and Derby, B., 2010, "Formation and Stability of Lines Produced by Inkjet Printing," Langmuir, **26**(12), pp. 10365-10372.

[29] Pataky, K., Braschler, T., Negro, A., Renaud, P., Lutolf, M.P., and Brugger, J., 2012, "Microdrop Printing of Hydrogel Bioinks into 3D Tissue-like Geometries," Adv. Mater., **24**, pp. 391-396.

[30] Pan, G., and Meng, H., 2001, "Experimental Study of Turbulent Mixing in a Tee Mixer Using PIV and PLIF," AIChE Journal, **47**(12), pp. 2653-2665.

[31] Hoffman, M., Schluter, M., and Rabiger, N., 2006, "Experimental Investigation of Liquid-liquid Mixing in T-shaped Micro-mixers Using μ-LIF and μ-PIV," Chemical Engineering Science, **61**, pp. 2968-2976.

[32] van Steijn, V., Kreutzer, M.T., and Kleijn, C.R., 2007, "μ-PIV Study of the Formation of Segmented Flow in Microfluidic T-junctions," Chemical Engineering Science, **62**, pp. 7505-7514.

[33] Kinoshita, H., Kaneda, S., Fujii, T., and Oshima, M., 2006, "Three-dimensional Measurement and Visualization of Internal Flow of a Moving Droplet Using Confocal Micro-PIV," Lab Chip, **7**, pp. 338-346.

[34] Castrejon-Pita, J.R., Betton, E.S., Kubiak, K.J., Wilson, M.C.T., and Hutchings, I.M., 2011, "The Dynamics of the Impact and Coalescence of Droplets on a Solid Surface," Biomicrofluidics, **5**, 014112.

[35] Bennacer, R., and Sefiane, K., 2016, "Proper Orthogonal Decomposition (POD) Analysis of Flow Structure in Volatile Binary Droplets," International Communications in Heat and Mass Transfer, **71**, pp. 172-175.

[36] Thielicke, W., and Stamhuis, E.J., 2014, "PIVlab – Towards User-friendly, Affordable and Accurate Digital Particle Image Velocimetry in MATLAB," Journal of Open Research Software, **2**(1), e30.

[37] Mirsepassi, A., and Ranking, D.D., 2014, "Particle Image Velocimetry in Viscoelastic Fluids and Particle Interaction Effects," Experiments in Fluids, **55**(1), pp. 1641.

[38] Rein, M., 1993, "Phenomena of a Liquid Drop Impact on Solid and Liquid Surfaces," Fluid Dynamics Research, **12**, pp. 61-93.

[39] Harlow, F.H., and Shannon, J.P., 1967, "The Splash of a Liquid Drop," Journal of Applied Physics, **38**, pp. 3855-3866.

[40] Ferreira, A.G., and Singer, M.J., 1985, "Energy Dissipation for Water Drop Impact into Shallow Pools," Soil Sci. Soc. Am. J., **49**, pp. 1537-1542.

[41] Zhang, Z., Xiong, R., Corr, D., and Huang, Y., 2016, "Study of Impingement Types and Printing Quality during Laser Printing of Viscoelastic Alginate Solutions," Langmuir, 32(12), pp. 3004-3014.

[42] Yarin, A.L., and Weiss, D.A., 1995, "Impact of Drops on Solid Surfaces: Self-Similar Capillary Waves, and Splashing as a New Type of Kinematic Discontinuity," J. Fluid Mech., **283**, pp. 141-173.

[43] Jayaratne, O.W., and Mason, B.J., 1964, "The Coalescence and Bouncing of Water Drops at an Air/Water Interface," Proceedings of the Royal Society of London, Series A, Mathematical, Physical and Engineering Sciences, **280**(1383), pp. 545-565.

[44] Kim, H.S., 1990, "A Kinetic Study on Calcium Alginate Bead Formation," Korean J. Chem. Eng., **7**, pp. 1-6.

[45] Braschler, T. Valero, A., Colella, L., Pataky, K., Brugger, J., and Renaud, P., 2011, "Link between Alginate Reaction Front Propagation and General Reaction Diffusion Theory," Anal. Chem., **83**, pp. 2234–2242.

[46] Li, L., Davidovich, A.E., Schloss, J.M., Chippada, U., Schloss, R.R., Langrana, N.A., and Yarmush, M.L., 2011, "Neural Lineage Differentiation of Embryonic Stem Cells within Alginate Microbeads," Biomaterials, **32**, pp. 4489–4497.

[47] Wang, J.H., 1953, "Tracer-diffusion in Liquids: IV. Self-Diffusion of Calcium Ion and Chloride Ion in Aqueous Calcium Chloride Solutions, J. Am. Chem. Soc., **75**, pp. 1769–1770.

[48] Morris, E.R., Rees, D.A., Thom, D., and Boyd, J., 1978, "Chiroptical and Stoichiometric Evidence of a Specific, Primary Dimerisation Process in Alginate Gelation," Carbohydr. Res., **66**, pp. 145–54.

[49] Xu, C., Zhang, Z., Christensen, K., Huang, Y., Fu, J., and Markwald, R.R., 2014, "Freeform Vertical and Horizontal Fabrication of Alginate-Based Vascular-Like Tubular Constructs Using Inkjetting," Journal of Manufacturing Science and Engineering, **136**(6), 061020.

Study of Layer Formation during Droplet-based 3D Printing of Gel Structures

Kyle Christensen, Yong Huang

List of Figures

Fig. 6. Schematic of diffusion process during printing.

Fig. 7. (a) A single-layer alginate sheet printed into a Laponite bath (experimental scenario B) to allow for clear visualization of interfaces between adjacent lines (inset: a magnified view illustrating key printing conditions for the deposition of printed lines L1-L4), and (b) identification of an interface and the coalescence distance L between two adjacent lines. Unspecified scale bars are 200 μm.

Fig. 8. Global and top view illustrations of the deposition and gelation of two adjacent printed lines and the formation of an interface. (a) Droplets are deposited along a printed line, where they coalesce within a fluid region (blue), (b) the printhead feeds to begin printing the adjacent line, while gelation (gray) trails behind the deposition site, and (c) as deposition of the adjacent line continues, the previously printed line becomes fully gelled and coalescence is prevented, forming an interface. Parameters shown: printhead travel speed v_{print}, feed distance d_{feed}, printhead feed speed v_{feed}, and coalescence distance L.

Fig. 9. Predicted gelation front location G(t) through the layer thickness as a function of time.

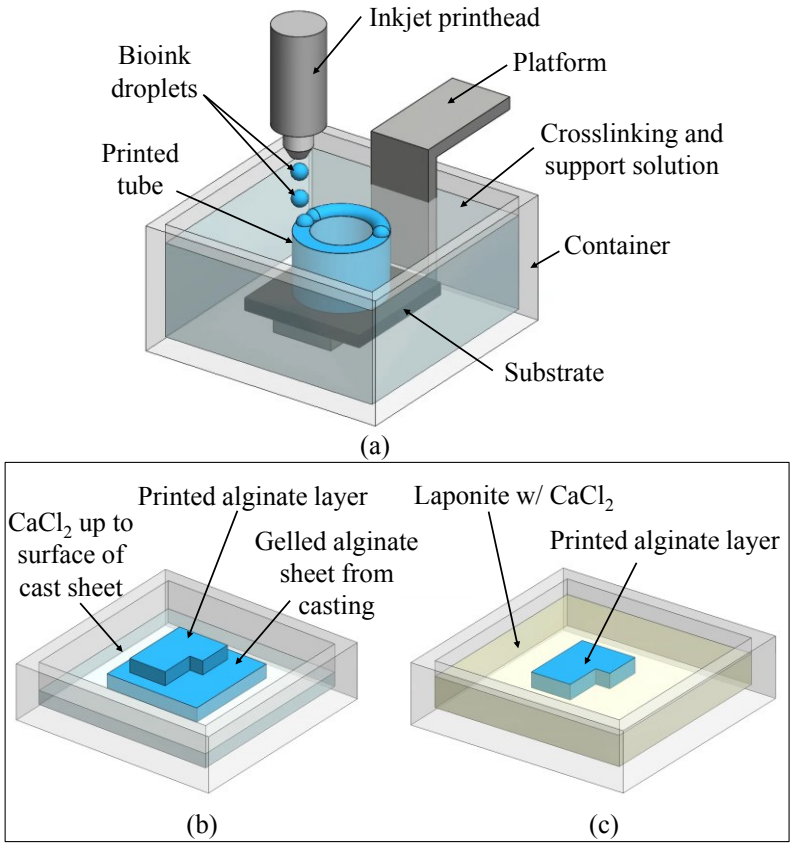

Fig. 1. (a) Typical inkjet printing setup, (b) experimental scenario A for the study of the layer formation process during the fabrication of single layers, and (c) experimental scenario B for the fabrication of single layers which are more easily imaged (used herein for illustration purposes only).

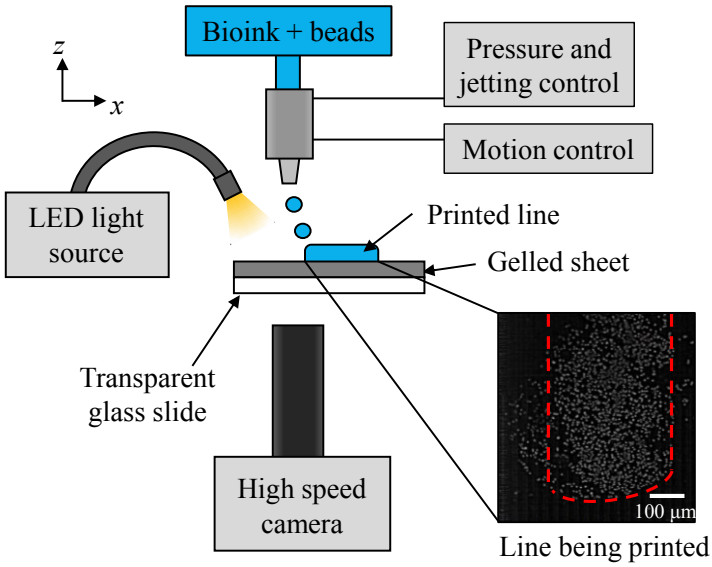

Fig. 2. Schematic of the high speed imaging setup with an inset showing a printed line (outlined by red dashes) containing microbeads for PIV analysis.

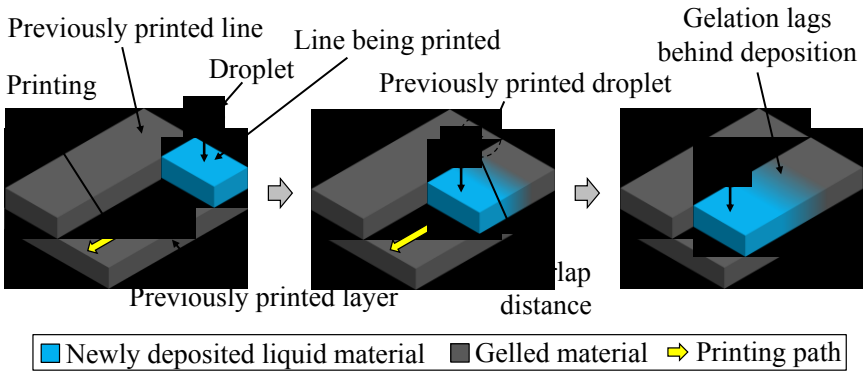

Fig. 3. Illustration of a typical layer formation process. Blue represents newly deposited liquid regions while gray represents gelled regions.

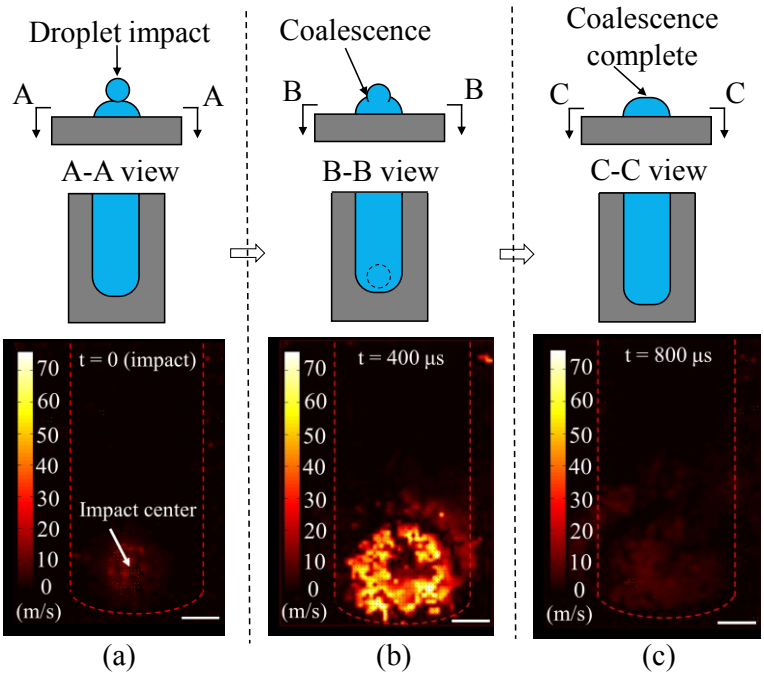

Fig. 4. (a)-(c) Schematic representations of front and top views and velocity magnitude color maps (m/s) at successive time points during the impact and coalescence of a droplet within a printed line. The primary printed line region is indicated by the red dashed line (scale bars: 100 µm).

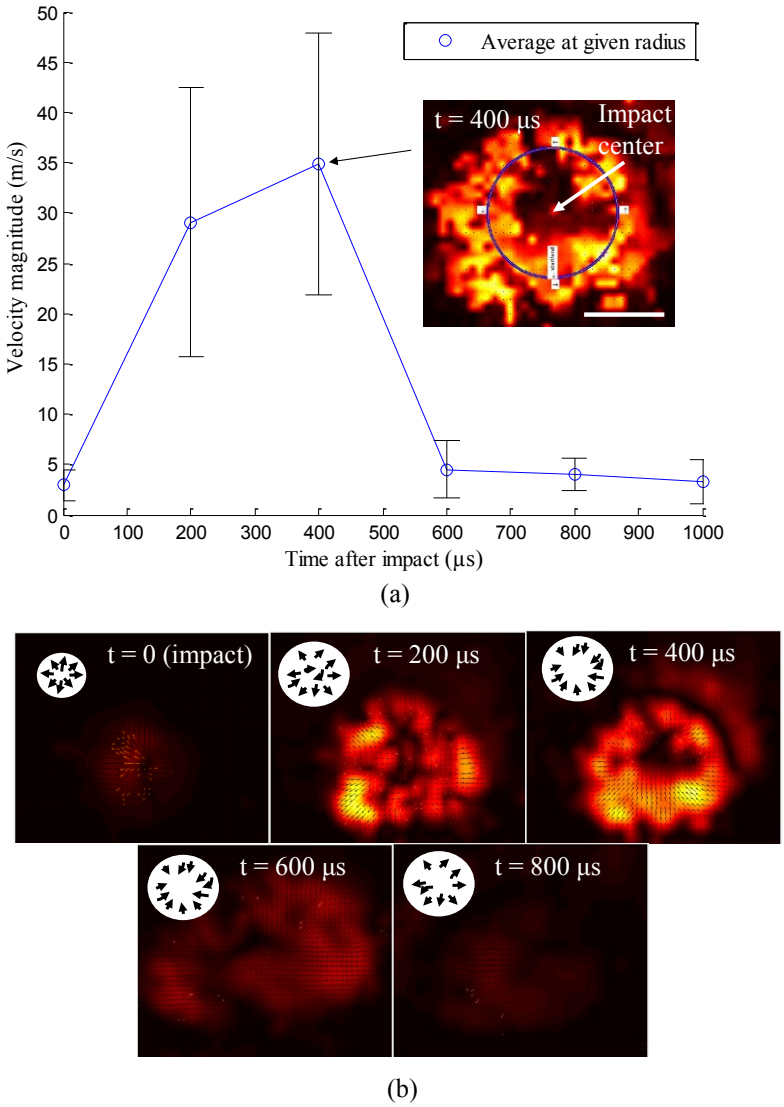

Fig. 5. (a) Average velocity as a function of time during the impact and coalescence of a droplet within a printed line (inset: PIV color map of velocity magnitude; scale bar: 100 µm) and (b) time evolution of velocity with insets representing simplified interpretations of the vector fields.

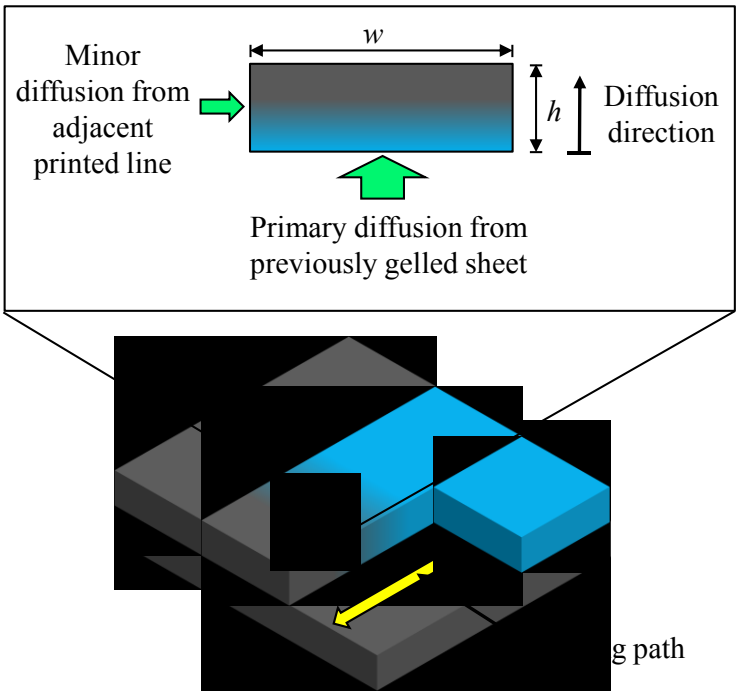

Fig. 6. Schematic of diffusion process during printing.

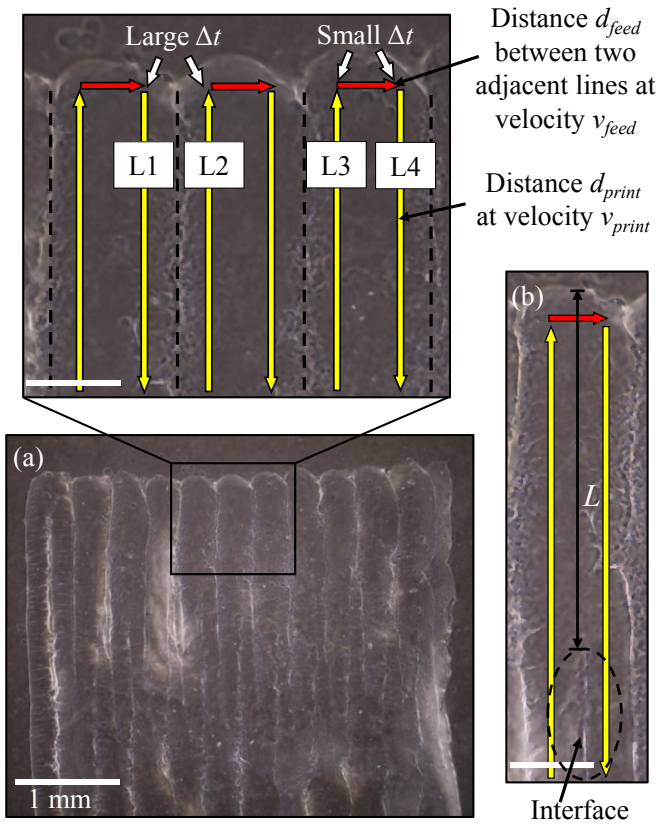

Fig. 7. (a) A single-layer alginate sheet printed into a Laponite bath (experimental scenario B) to allow for clear visualization of interfaces between adjacent lines (inset: a magnified view illustrating key printing conditions for the deposition of printed lines L1-L4), and (b) identification of an interface and the coalescence distance L between two adjacent lines. Unspecified scale bars are 200 μm.

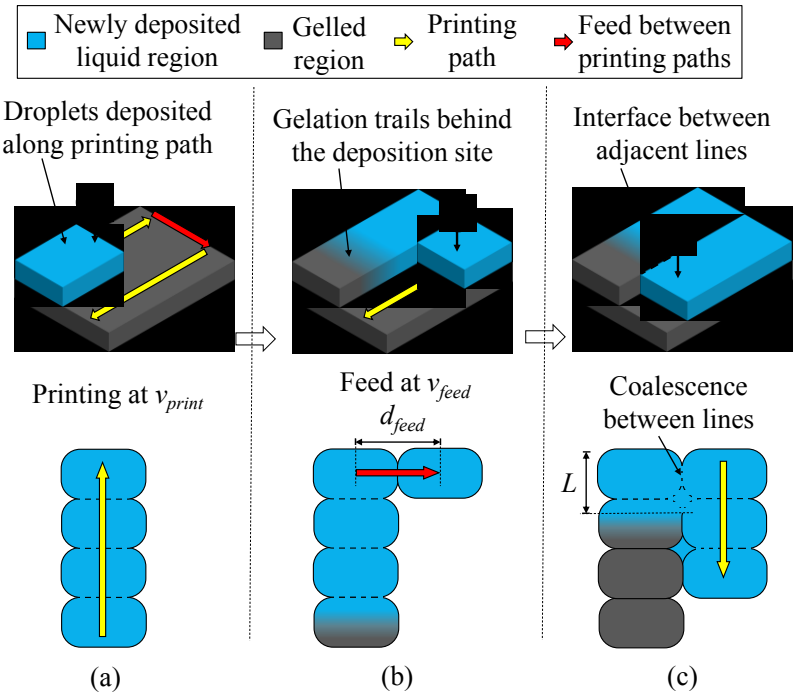

Fig. 8. Global and top view illustrations of the deposition and gelation of two adjacent printed lines and the formation of an interface. (a) Droplets are deposited along a printed line, where they coalesce within a fluid region (blue), (b) the printhead feeds to begin printing the adjacent line, while gelation (gray) trails behind the deposition site, and (c) as deposition of the adjacent line continues, the previously printed line becomes fully gelled and coalescence is prevented, forming an interface. Parameters shown: printhead travel speed v_{print}, feed distance d_{feed}, printhead feed speed v_{feed}, and coalescence distance L.

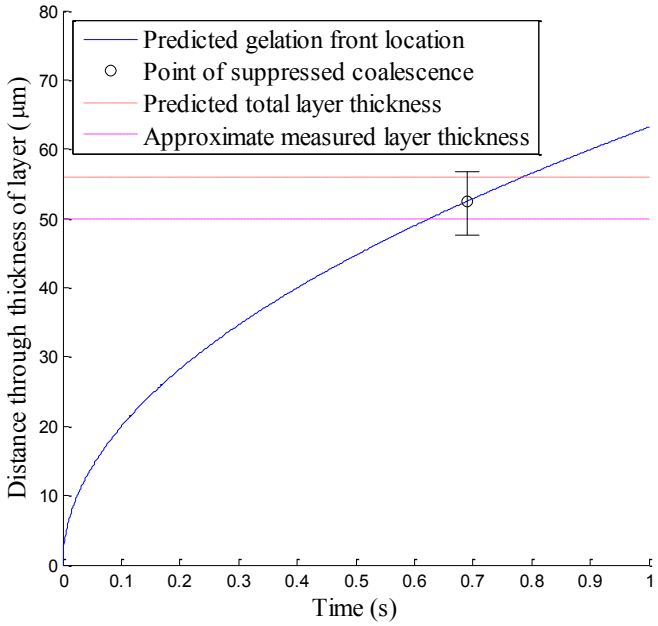

Fig. 9. Predicted gelation front location *G(t)* through the layer thickness as a function of time.